*Acta of Bioengineering and Biomechanics*
*Vol. 27, No. 3, 2025*

Original paper
DOI: 10.37190/abb/210002

sciendo

# Impact of bileaflet mechanical heart valve implantation angle on left ventricular hemodynamics and blood cell damage

ZHIXIONG LI[1], YAN QIANG[1]*, LIANG QI[2], JIABAO QI[1], WENYU GENG[1]

[1] The College of Energy and Power Engineering, Lanzhou University of Technology, Langongping Road, Lanzhou, China.
[2] Cardiovascular Surgery, The First Hospital of Lanzhou University, Chengguan District, Lanzhou, China.

*Purpose*: The implantation angle of Bileaflet Mechanical Heart Valve (BMHV) is critical issue in valve replacement surgery. Investigating the local hemodynamic characteristics and analyzing the postoperative flow dynamics can provide valuable insights for determining the optimal implantation angle, thereby offering clinical guidance for improved surgical outcomes. *Methods*: Three-dimensional anatomical model of the Left Ventricle (LV) and BMHV was reconstructed based on patient-specific medical imaging data and anatomical parameters. The hemodynamic effects of varying implantation angles were investigated using Computational Fluid Dynamics (CFD) integrated with a Fluid-Structure Interaction (FSI) framework. *Results*: The key analyses focused on the downstream shear stress distribution, vortex dynamics, clinically relevant hemodynamic indicators. When the valve was implanted along the axis of the aortic outflow tract (referred to as the AO angle), several benefits were observed. Blood flow penetrability improved, high shear stress regions were reduced, mechanical trauma to blood cells was significantly lessened. Quantitative metrics further demonstrated that the AO angle minimized values of Time-Averaged Wall Shear Stress (TAWSS), Oscillatory Shear Index (OSI) and Relative Residence Time (RRT). These metrics indicate more stable hemodynamics and a lower risk of ventricular wall inflammation and thrombosis. Furthermore, the Hemolysis Index (HI) reached its lowest level under the AO angle, suggesting optimal mitigation of hemolysis. This study systematically examines how the orientation of BMHV implantation affects LV hemodynamics. It identifies the AO angle as the most effective strategy for positioning. *Conclusions*: These findings provide quantitative evidence that can inform preoperative planning and support the advancement of precision-guided cardiac valve interventions based on hemodynamics considerations.

*Key words*: *left ventricle, Bileaflet Mechanical Heart Valve, implantation angle, hemodynamics, blood cell damage*

## 1. Introduction

The implantation of Bileaflet Mechanical Heart Valve (BMHV) is one of the main treatments for severe heart valve diseases, as BMHVs are widely utilized in clinical practice, with over 80% of mitral valve (MV) replacement procedures involving their use [4], [31]. Researches indicates that the angle at which BMHVs are implanted can significantly affect the hemodynamic characteristics within the Left Ventricle (LV), including vortex formation, shear stress distribution, and energy loss, all of which influence cardiac function [11], [22]. Correctly positional the valve can reduce flow turbulence, enhance the forward flow of blood, and lessen the workland on the LV [16].

Current investigations used a combination of Computational Fluid Dynamics (CFD), *in vitro* experiments and clinical data to clarify how different implantation angles affect LV blood flow. Choi [6] applied CFD simulations to investigate intraventricular flow at different implantation angles, their findings indicated that an optimal orientation promotes smoother blood flow while minimizing regurgitation and turbulence. Machler [18] found that aligning the angle of the BMHV with the natural direction of blood flow at the MV significantly improves blood flow efficiency and reduces pressure and load on the LV [34]. Murty [20] examined the blood

* Corresponding author: Yan Qiang, The College of Energy and Power Engineering, Lanzhou University of Technology, Langongping Road, Lanzhou, China. E-mail: 20070046@lut.edu.cn
Received: June 3rd, 2025
Accepted for publication: August 28th, 2025

flow characteristics of BMHV at different angles using animal models. They found that even minor angular deviations could significantly affect the heart's pumping efficiency. These findings have been supported by clinical studies showing that patients with ideal implantation orientations consistently demonstrated better cardiac function compared to those with suboptimal placements [14], [32].

These studies collectively indicated that variations in angle of valve implantation can alter intraventricular flow patterns within the LV, thereby affecting the distribution of blood flow and potentially inducing blood cell damage. Studies have shown that mechanical hemolysis is not only related to the absolute level of shear stress but also closely associated with the cumulative effect of stress duration [26], [29], [35]. Qiang et al. [23], [24] conducted a combination of numerical simulations and *in vitro* experiments to investigate the distribution characteristics of shear stress, Time-Averaged Wall Shear Stress (TAWSS), Oscillatory Shear Index (OSI) and Relative Residence Time (RRT) downstream of BMHV. They found that the shapes and opening-closing modes of BMHV significantly impact cell damage within the ventricle, contributing to hemolysis, thrombosis, and other pathological issues.

In the studies mentioned, most of the implantation angles examined were either AO or AAO (Anti-Anatomical position), which do not represent the full range of clinically observed implantation scenarios. Additionally, existing research has primarily concentrated on how valve orientation affects flow patterns, without adequately addressing how implantation angle impacts blood damage and related hemocompatibility issues. This paper primarily employs CFD, specifically to investigate the impact of four different valve implantation angles on key medical evaluation indices. This study not only offers a high-precision prediction tool for preoperative planning but also aims to reduce the risk of thrombosis caused by abnormal shear forces. Ultimately, this may decrease postoperative anticoagulation treatment dependence, improve patient outcomes, and alleviate the economic burden on healthcare systems.

# 2. Materials and methods

## 2.1. Left ventricle and BMHV implantation angle model

Based on the patient's Computed Tomography (CT) images, a high-precision 3D model of the LV was constructed using multi-region masking segmentation technology. This method enables accurate segmentation and labeling of different anatomical structures such as the left atrium, left ventricle and aorta, followed by geometric optimization through trimming, wrapping, smoothing, and Boolean operations [36]. In this paper, the impact of leaflet implantation angles on the blood flow characteristics within the LV was primarily investigated. Physiological parameters of the human body were controlled by inlet and outlet boundary conditions, and the models of the left atrium and aorta were simplified, as shown in Fig. 1a–c. The leaflet model selected is one of the most commonly used BMHV models in clinical practice, with an annular inner diameter of 21.6 mm, a leaflet thickness of 1 mm, and rotation angles $\theta_{\min}$ and $\theta_{\max}$ of 25°and 85°, respectively. In Figure 1d, the positions of BMHV in both closed and open states are shown, with different implantation angles. The AO direction represents the anatomical direction, and Anterior Leaflet (AL) and Posterior Leaflet (PL) refer to the anterior and posterior leaflets, respectively. The early diastolic (E-wave) and atrial systolic (A-wave) waveforms are based on a simple harmonic oscillator (SHO) model that was validated by Doppler echocardiographic data [7], [9], [10] with the E/A ratio (EAR) set to 1.5. A heart rate of 75 beats per minute (BPM) and flow through the LV, $Q(t)$, were assumed (Fig. 1f). $Q(t)$) represents an idealized left ventricular inflow function, validated by echocardiographic data, and was used as one of the hemodynamic driving conditions to ensure that the model reflects the clinical processes of filling and ejection.

## 2.2. Computational fluid dynamics modelling

During the LV contraction process, the blood flow from the MV into the LV and then out through the aortic valve satisfies the laws of mass conservation and momentum conservation.

The continuity equation is as follows:

$$\frac{\partial \rho}{\partial t} + \nabla \cdot (\rho \mathbf{v}) = 0 , \tag{1}$$

where $\mathbf{v}$ represents the fluid velocity vector.

The momentum equation is as follows:

$$\frac{\partial(\rho u_i)}{\partial t} + \frac{\partial(\rho u_i u_j)}{\partial x_j} = -\frac{\partial p}{\partial x_i} + \frac{\partial}{\partial x_j}\left(\mu \frac{\partial u_i}{\partial x_j}\right) + \rho f_i, \tag{2}$$

where: $\rho$ is the fluid density; $t$ is time; $u_i$, $u_j$ are the three-dimensional velocity components in the $i$ and $j$

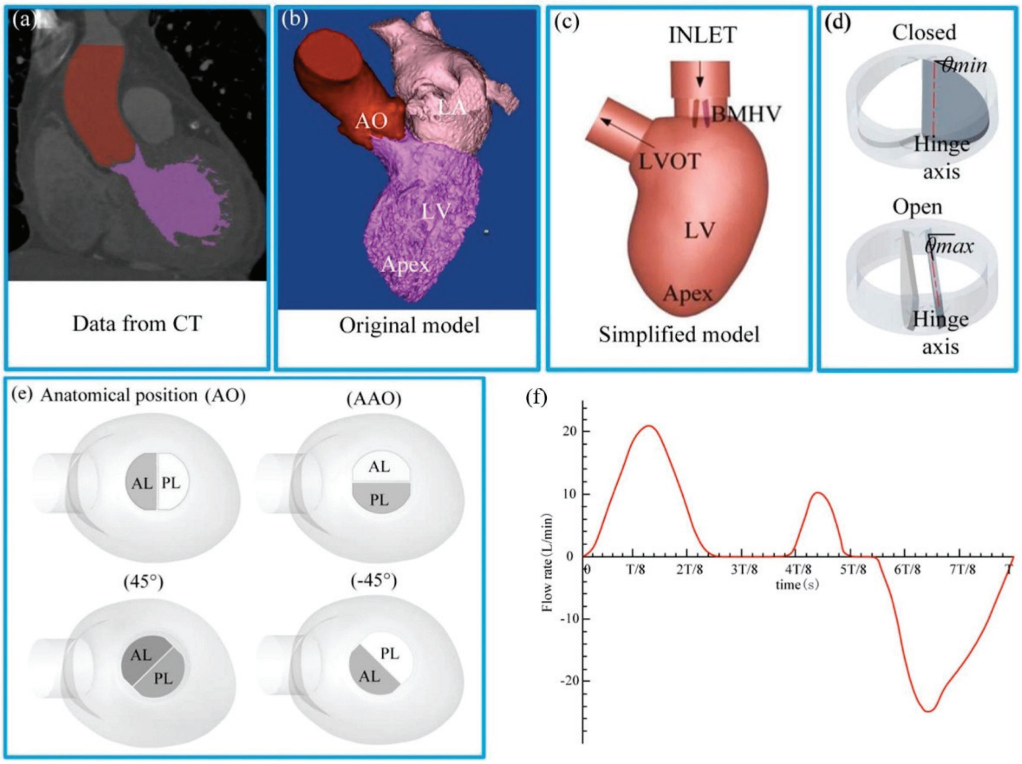


Fig. 1. Left Ventricular Model with BMHV Implantation Angles. (a) Contrast CT scan data of the normal human heart. The left heart is highlighted, (b) LV model reconstructed from contrast CT scan data, LA: left atrium, AO: aorta, (c) simplified computational model, LVOT: LV outflow tract, BMHV: bileaflet mechanical heart valve, (d) BMHV in the closed and open positions (angles $\theta_{\min}$ and $\theta_{\max}$, respectively), and four valve orientations investigated in this study and how the axes of the anterior and posterior leaflets (AL and PL, respectively) are rotated, (e) axial view of the left atrium and LV

directions ($i$ = 1, 2, 3; $j$ = 1, 2, 3); $p$ is pressure; $\mu$ is the dynamic viscosity coefficient of the fluid; $f_i$ is the body force in the $i$ direction.

Blood flow within the LV exhibits typical turbulent characteristics, with flow patterns that include vortex structures, high complexity, and three-dimensional unsteady features [28]. In this study, numerical simulations were performed using ANSYS Fluent software, with pressure boundary conditions applied at both the inlet and outlet. The inlet pressure was prescribed based on Doppler echocardiography data, while the outlet pressure waveform was defined according to the physiological variation of aortic pressure, thereby ensuring consistency between the simulation results and clinical conditions. The opening and closing sequence of the LV inlet was controlled through events: during diastole, the LV wall expands, the inlet opens, and blood enters the LV, acting on the BMHV and causing it to open. During systole, the LV wall contracts, the outlet opens, blood flow drives the closure of the BMHV, and blood is ejected into the aorta, thus ensuring unidirectional flow. In this study, the Reynolds-averaged simulation method was employed to solve the transport equations for turbulent kinetic energy $k$ and specific dissipation rate $\omega$, ensuring simulation accuracy while controlling computational costs. Specifically, the SST $k$-$\omega$ turbulence model was selected, as it accurately represents the turbulent shear stress transport mechanism within the left ventricle's reverse pressure gradient boundary layer, particularly suitable for predicting flow separation phenomena caused by reverse pressure gradients, thus precisely describing hemodynamic behavior [1].

This paper develops a numerical model for simulating incompressible blood flow within the LV using a pressure-based solver. To address mesh distortion caused by the high-frequency opening and closing of the valve as well as pulsatile flow effects, the Pressure Implicit with Splitting of Operators (PISO) decoupled iterative algorithm was employed, combined with a node-based Green–Gauss gradient discretization scheme [1], [27]. Given the rapid periodic motion of the BMHV, the PRESTO! pressure interpolation scheme was adopted to improve interface capturing accuracy [21]. When analyzing intraventricular hemodynamics influenced by BMHV, it is essential to manage the complex coupling between dynamic deformation and flow. Therefore, a bidirectional Fluid–Structure Interaction (FSI) framework was established to simultaneously solve the leaflet kinematics and the systolic-diastolic motion of the ventricular wall, ensuring that dynamic parameters at the inlet and outlet boundaries strictly comply with physiological standards of the human body.

## 2.3. Data analysis methods

Several metrics were used to quantitatively analyze the blood flow patterns within the LV. The velocity gradient tensor can be decomposed into the following two components.

$$\frac{\partial \mathbf{u}_i}{\partial x_j} = \frac{1}{2}\left[\frac{\partial \mathbf{u}_i}{\partial x_j} + \frac{\partial \mathbf{u}_j}{\partial x_i}\right] + \frac{1}{2}\left[\frac{\partial \mathbf{u}_i}{\partial x_j} - \frac{\partial \mathbf{u}_j}{\partial x_i}\right]. \tag{3}$$

The symmetric part, denoted as $S_{ij}$, is often referred to as the strain rate tensor, and the antisymmetric part, denoted as $\Omega_{ij}$, is often referred to as the rotation rate or vortex tensor.

$$S_{ij} = \frac{1}{2}\left[\frac{\partial \mathbf{u}_i}{\partial x_j} + \frac{\partial \mathbf{u}_j}{\partial x_i}\right], \quad \Omega_{ij} = \frac{1}{2}\left[\frac{\partial \mathbf{u}_i}{\partial x_j} - \frac{\partial \mathbf{u}_j}{\partial x_i}\right]. \tag{4}$$

The second invariant $Q$ of the velocity gradient tensor was defined to analyze vortex structures [15]. $Q$ is a mathematical quantity commonly used in fluid dynamics to identify and extract vortex structures.

$$Q = \frac{1}{2}(\Omega_{ij}\Omega_{ij} - S_{ij}S_{ij}). \tag{5}$$

Studies have shown that when the Wall Shear Stress (WSS) is too low, it may trigger inflammatory responses in endothelial cells and promote platelet deposition, while excessively high WSS may induce platelet activation, thereby damaging the ventricular wall [19]. TAWSS represents the average WSS over the entire cardiac cycle and is used to comprehensively assess the overall hemodynamic force exerted on the vessel wall. When the value of TAWSS falls below the normal range, it indicates that the endothelium has been subjected to prolonged low shear stress, which can lead to endothelial cell injury.

$$\text{TAWSS} = \frac{1}{T}\int_0^T |\bar{\tau}_w|\, dt, \tag{6}$$

where $|\bar{\tau}_w|$ is the WSS vector, and $T$ is the cardiac cycle duration.

OSI is used to quantify the instability of blood flow. It reflects the degree of turbulence and oscillation in WSS within the bloodstream. A high OSI value indicates pronounced disturbances and WSS fluctuations in a given region, suggesting unstable blood flow. This instability may lead to inflammation and damage of the vessel wall.

$$\text{OSI} = \frac{1}{2}\left(1 - \frac{\left|\int_0^T \vec{\tau}_w\, dt\right|}{\int_0^T |\vec{\tau}_w|\, dt}\right). \tag{7}$$

RRT characterizes the duration of blood residence near the vessel wall during its interaction with it. It reflects how flow direction changes – especially around vascular stenoses or abnormal wall regions – affect the inner vascular layer. An increased RRT value indicates prolonged blood residence in these critical regions, which can alter both the number and activity of receptors on endothelial cell surfaces. This may ultimately trigger various physiological and pathological responses, such as endothelial cell proliferation, apoptosis, or migration [33].

$$\text{RRT}(s) = \frac{1}{(1 - 2\text{OSI})\text{TAWSS}}. \tag{8}$$

Hemolysis refers to the phenomenon where red blood cells release hemoglobin into the plasma due to mechanical damage to their membranes. Hemolysis occurs when the shear stress acting on red blood cells and the exposure time exceed certain thresholds. Studies have shown that the degree of hemolysis follows a power-law relationship with both shear stress and exposure duration [8]. The Hemolysis Index (HI) is a dimensionless parameter commonly used to quantify the amount of hemolysis, and it is defined by the following equation [12]:

$$\text{HI}(\%) = 1.80 \times 10^{-6} \times \tau^{1.991} \times \Delta t^{0.765}, \tag{9}$$

where: $\tau$ represents the scalar shear stress, and $\Delta t$ denotes the exposure time of red blood cells under the shear stress $\tau$.

$$\tau = \left[\frac{1}{6}\sum(\tau_{ii} - \tau_{jj})^2 + \sum \tau_{ij}^2\right]^{1/2}, \tag{10}$$

where: $\tau_{ij}$ represents the shear stress tensor, and HI is calculated over a complete cardiac cycle.

# 3. Results

In summary, the study on different implantation angles of BMHV demonstrates that the implantation angle significantly alters the intraventricular flow patterns of the LV. When the valve is implanted at the AO angle, vortex evolution within the LV consumes less energy, thereby reducing myocardial oxygen consumption and mechanical load. The blood flow penetration capability is enhanced, transport efficiency is improved, and regions of high WSS concentration are narrower and of lower intensity, which reduces the risk of blood cell damage.

Based on medical evaluation metrics, AO-angle implantation results in lower TAWSS at the annulus, more stable flow, smaller values of RRT and a lower risk of thrombosis. The HI is also the lowest, indicating minimal blood cell damage and the lowest risk of hemolysis. Therefore, AO-angle implantation is recommended as the optimal approach for patients undergoing mechanical valve replacement.

# 4. Discussion

A comparative analysis was conducted on the impact of different mechanical valve implantation angles on LV blood flow characteristics. All data were derived from four characteristic instants within a complete cardiac cycle. These include: (i) End of the diastolic phase E-wave acceleration at 0.105 s, (ii) Peak of the E-wave during diastole at 0.2 s, (iii) End of the E-wave during diastole at 0.3 s, (iv) Interval between the E-wave and A-wave at 0.45 s.

## 4.1. The law of vortex evolution

Vorticity refers to the curl of the fluid velocity vector and is used to quantify the magnitude and direction of vortices. As shown in Fig. 2, the vorticity field within the left ventricular cavity is visualized using the $Q$-criterion, which enables the extraction of three-dimensional vortex features. Through this method, the generation, growth, breakdown, and dissipation of vortex rings can be clearly observed.

During the acceleration phase of the E-wave in diastole (Fig. 2i), numerous vortical structures are observed at the left ventricular outflow tract (LVOT) in the AO anatomical orientation, indicating that residual vortices from systole persist into early diastole. In contrast, other implantation angles show minimal or no vortices in early diastole, suggesting that systolic vortices have completely dissipated, resulting in greater energy loss. At the peak of the E-wave (Fig. 2ii), a “front vortex” forms below the anterior leaflet, mainly near the aortic sinus, and a “rear vortex” forms below the posterior leaflet. As the central orifice widens, its jet stream strengthens, and the central vortex elongates. The figure clearly shows that the vortex motion direction at peak E-wave varies significantly depending on the implantation angle. In the AO orientation, the front vortex moves in line with the outflow direction, which helps reduce blood-wall collisions, leading to lower energy loss. By the end of the E-wave (Fig. 2iii), the rear vortex grows faster and evolves into a rotational vortex. This rotational structure drives blood from the apex upward, which increases flow turbulence near the apex, thereby reducing blood residence time and lowering thrombosis risk. Notably, in the AO orientation, the rotational vortex aligns with the aortic direction, more effectively propelling blood toward the outflow, resulting in higher pumping efficiency than other implantation directions.

During the interval between the E-wave and A-wave (Fig. 2iv), the inlet flow through the mechanical valve drops to zero. At this stage, the large-scale vortices generated during the E-wave begin to dissipate and break down. Notably, under the AO implantation orientation, fewer residual vortical structures are observed in the LV compared to other orientations, indicating more efficient vortex clearance. Analyzing the entire diastolic filling process, it becomes evident that the AO implantation angle offers hemodynamic characteristics more aligned with physiological flow patterns. In contrast, non-AO orientations are more likely to cause flow stagnation near the ventricular apex, which in turn elevates the risk of thrombus formation due to prolonged blood residence time in low-shear regions.

## 4.2. Hemodynamic medical evaluation metrics

Prolonged exposure of ventricular endothelial cells to abnormal shear stress can lead to dysfunction and trigger inflammatory diseases [17]. To better differentiate the effects of various valve implantation angles on the ventricular wall, this paper employs several hemodynamic medical evaluation metrics, including TAWSS, OSI, and RRT.

As shown in Fig. 3, the TAWSS distribution on the left ventricular surface is analyzed under four different BMHV implantation angles. Existing studies define regions with TAWSS values below 0.4 Pa as low WSS

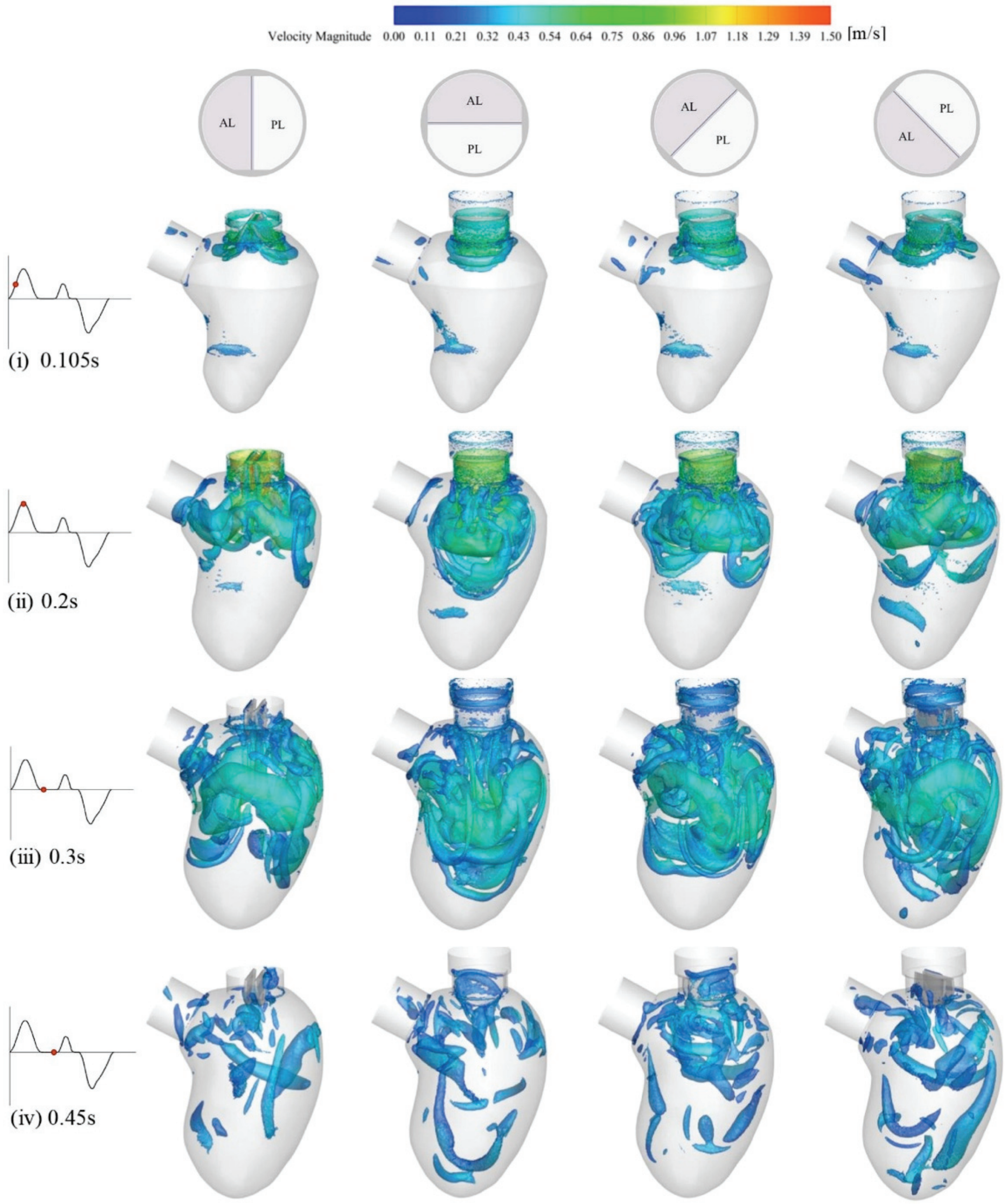


Fig. 2. The vorticity at characteristic moments of a cardiac cycle is identified using the isosurface $Q$ criterion ($Q > 1000$). The second row shows four different implantation angles of the BMHV. (i) The accelerated phase of the E wave during diastole at 0.105 s, (ii) the peak of the E wave during diastole at 0.2 s, (iii) the end of the E wave during diastole at 0.3 s, (iv) the interval between the E wave and A wave at 0.45 s

zones and those above 5 Pa as high WSS zones [5], [25]. A comparative analysis across the four conditions reveals that the low shear stress zones are mainly located in the middle and lower parts of the LV. For the AO direction, influenced by the jet flow from the two lateral orifices and the evolution of left and right vortices within the ventricle, the high WSS zone is primarily found in the middle of the septal side and the upper part of the lateral wall. The shear stress value exceeds 5 Pa at the inlet valve ring, with the highest shear stress occurring at the hinge of the leaflet and below the leaflet. For the AAO direction, due to the effect of jet flow and abnormal vortices, a large high WSS area appears in the upper sections of the inferior and anterior walls, with a peak value above 5 Pa. The shear stress at the valve ring shows abnormal extreme values, which can easily induce platelet activation and cause significant blood cell damage, thereby increasing the risk of thrombosis [2]. For the 45° and –45° directions, the high shear stress regions are mainly concentrated

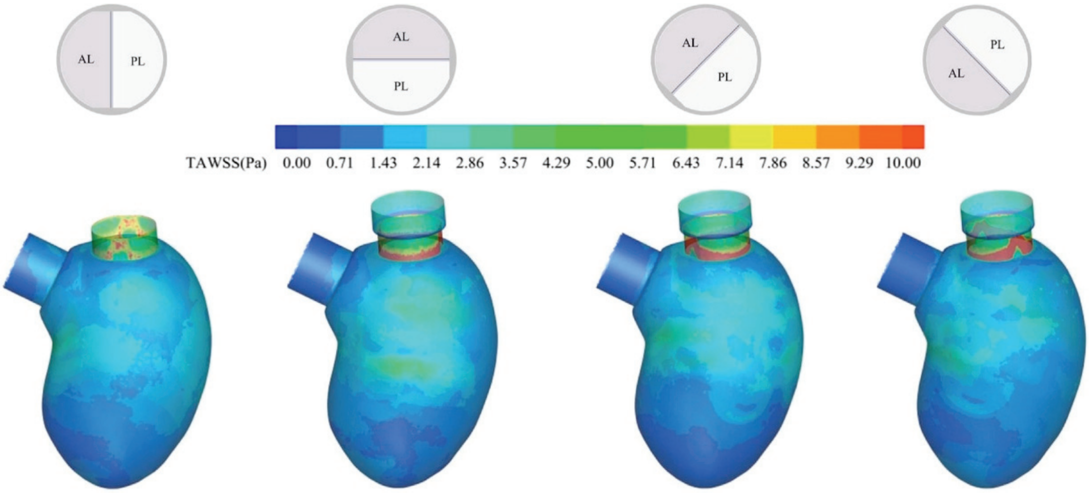


Fig. 3. TAWSS distributions are presented with the ventricular wall rendered semi-transparent.
The first row illustrates the four different BMHV implantation angles.
The third row shows the TAWSS distribution under different implantation angles

in the lower lateral wall and the middle-upper part of the anterior septal side, with similar findings to the AAO direction. At the valve ring, shear stress again presents abnormal extreme values. These findings suggest that different implantation angles of the mechanical valve lead to different distributions of high shear stress zones. The AO direction presents a lower risk of thrombosis formation at the valve ring compared to other implantation angles.

OSI reflects the instability of blood flow and is commonly used to evaluate the axial variation of shear stress. As shown in Fig. 4, the OSI distribution on the left ventricular wall for different implantation angles of the valve leaflets is presented. When the OSI approaches 0, blood flow tends to be unidirectional shear flow; when the OSI approaches 0.5, the blood flow oscillates more significantly [13]. Comparing the OSI distribution on the ventricular wall under the four implantation conditions, it is observed that due to the complex blood flow patterns within the ventricle, the blood flow is highly unstable, with high OSI regions showing irregular patterns and wide distribution, almost covering all areas of the left ventricular wall. In the AO direction, the OSI at the apex is close to 0, and the low OSI region at the apex is noticeably larger than those in other implantation angles. This is because the different implantation angles of the valve change the motion pattern of the ventricular jet, increasing the instability of the blood flow and raising the possibility of inflammation and damage to the ventricular wall [3].

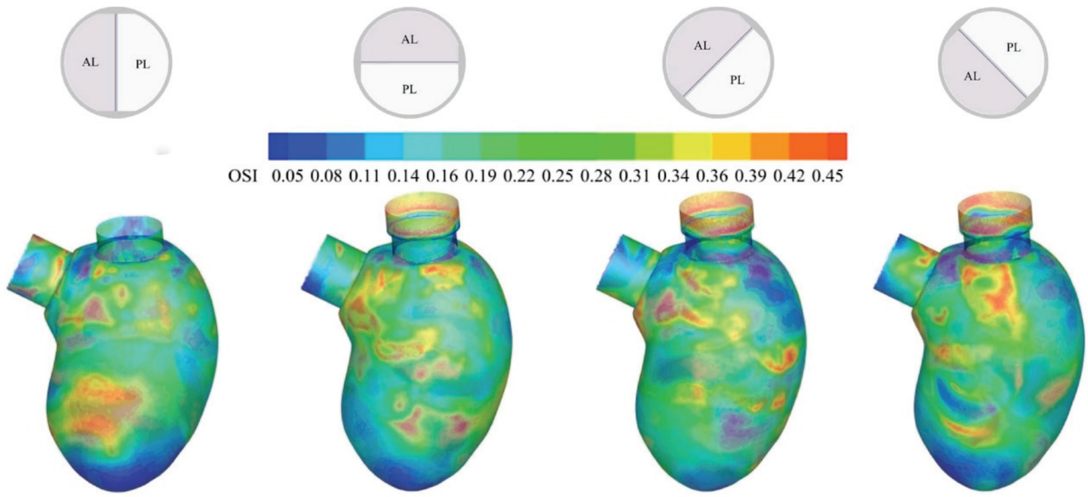


Fig. 4. The OSI evaluation metric with the ventricular wall surface rendered transparent.
The first row presents the four different implantation angles of the BMHV.
The third row shows the OSI distribution for each implantation angle

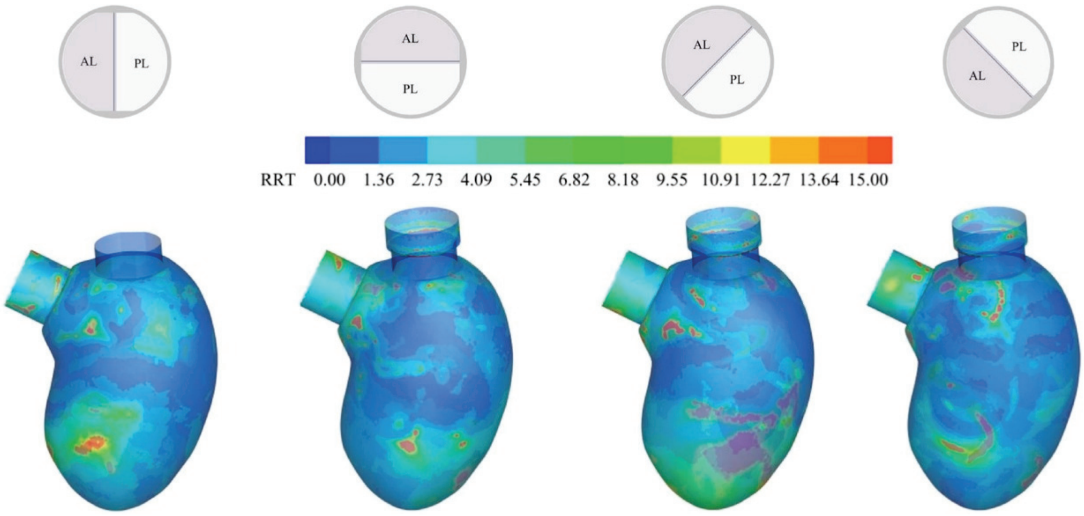


Fig. 5. The RRT evaluation metric, with the ventricular wall processed for transparency.
The first row represents the four different implant angles of BMHV.
The third row shows the RRT distribution for different implant angles

In the study of left ventricular blood flow characteristics at different valve implant angles, RRT represents the residence time of blood near the ventricular wall, reflecting the impact of changes in blood flow direction on the ventricular wall. RRT can be used to assess the risk of thrombosis formation [36]. As shown in Fig. 5a, the RRT distribution on the left ventricular wall for different implant angles is presented, with regions of higher RRT corresponding to areas of low shear stress and high OSI. Analyzing the RRT distribution on the left ventricular wall for the four implant angles, and influenced by jet vortices, the RRT values in the middle of the LV are relatively low, indicating better blood flow. High RRT regions are primarily concentrated near the aortic sinus and at the apex. This is because, during diastole, the jet blood moves downward, forming anterior and posterior vortices with opposite motion directions. The anterior vortex drives blood toward the outlet, and at the narrowing shape near the aortic sinus, the blood flow pattern becomes more complex, leading to an increased distribution of high RRT. Due to the weak blood penetration ability downstream of the bileaflet mechanical valve, the blood struggles to reach the apex, leading to blood stagnation at the apex and a higher distribution of RRT values there. For the AO direction, the high RRT regions are mainly concentrated on the posterior septal side in the middle-lower part. When the mechanical valve is implanted at a 45° angle, an abnormally high RRT region appears at the apex, which can easily lead to endothelial cell damage and increase the risk of thrombosis formation.

The downstream blood flow pattern of the bileaflet mechanical valve tends to generate higher shear stress, increasing the risk of red blood cell destruction. HI is selected as the evaluation indicator for hemolysis risk for different valve implantation models [30]. As shown in Fig. 6, the implantation orientation of the mechanical valve affects the HI in the ventricle. The HI value is the smallest when the valve is implanted at the AO orientation, while the HI value is the largest at the AAO orientation. The HI values for the 45° and –45° orientations are relatively close. This indicates that the implantation orientation of the mechanical valve affects the blood flow transport pattern in the ventricle, and abnormal flow increases the risk of hemolysis, with the lowest risk occurring at the AO orientation.

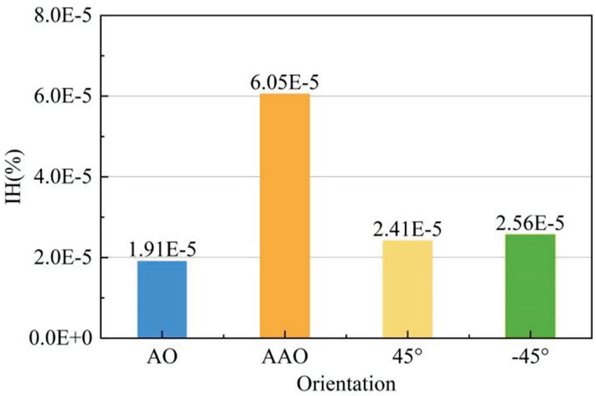


Fig. 6. Hemolysis index under different implantation orientations of mechanical heart valves

## 5. Conclusions

This study reconstructed a three-dimensional model of the LV based on clinical CT medical imaging and designed a bileaflet mechanical valve configuration according to cardiovascular fluid dynamics parameters. Using a multimodal fluid dynamics analysis approach, the study focused on revealing the vortex evolution characteristics of the flow field downstream of the bileaflet mechanical valve under different implantation angles. It systematically explained typical hemodynamic phenomena and their mechanisms under the valve-blood flow coupling effect. The results provide an important theoretical basis for optimizing clinical valve implantation plans and postoperative hemodynamic assessments.

The evolution of vortices reflects critical physiological changes in the left ventricle. When the valve is implanted at the AO angle, the energy consumption during the generation, growth, collapse, and dissipation of vortices in the LV is relatively low. However, when implanted at other angles, abnormal vortices alter the blood flow pattern in the ventricle, increasing myocardial oxygen consumption and mechanical load. Therefore, the treatment effect is better when the valve is implanted at the AO angle.

Medical evaluation indices are crucial in analyzing the hemodynamics within the LV. When analyzing the TAWSS distribution, the mechanical valve implantation angle influences the distribution of high shear stress regions. When the valve is implanted at the AO angle, the average value and variation range of TAWSS data on the left ventricular wall are smaller, resulting in a lower risk of thrombosis at the valve ring. From the OSI distribution, blood flow is more stable when implanted at the AO angle, while other implantation angles alter the blood flow pattern within the ventricle, increasing the instability of the blood flow and raising the possibility of inflammation and damage to the ventricle wall. Analyzing the RRT data characteristics, the RRT distribution in the mid-left ventricle is low, indicating good blood flow, influenced by jet vortices. Due to the weak blood flow penetration of the mechanical valve, the RRT distribution is higher at the apex. When analyzing the RRT distribution at different angles across various sections, the AO angle shows smaller averages and standard deviations. When the valve is implanted at a 45° angle, an abnormally high RRT region appears at the apex, which easily leads to damage to the endothelial cells within the ventricle and thrombosis formation. The valve implantation angle affects the hemolysis risk within the ventricle, with the AO angle implantation resulting in the lowest HI value, indicating the minimal hemolysis risk.

## Acknowledgements

This work was supported in part by the National Natural Science Foundation of China (No. 52366003).

## References

[1] ANSYS Inc. ANSYS Fluent Theory Guide[M]. Canonsburg: ANSYS Inc., 2018.

[2] Bluestein D., *Flow-induced platelet activation and damage accumulation in a mechanical heart valve: Numerical studies*, Artificial Organs, 2013, 37 (10), 888–896.

[3] Borazjani Iman., *The Effect of Implantation Orientation of a Bileaflet Mechanical Heart Valve on Kinematics and Hemodynamics in an Anatomic Aorta*, Journal of Biomechanical Engineering, 2010, 132 (11), 111005.

[4] Bourguignon T., Bouquiaux-Stablo A.L., Candolfi P., Mirza A., Loardi C., May M.A., *Very Long-Term Outcomes of the Carpentier-Edwards Pericardial Valve in Aortic Position*, The Annals of Thoracic Surgery, 2018, 105 (3), 816–822.

[5] Bourquelot P., Gaudric J., Turmel-Rodrigues L., Franco G., Laere O.V., Raynaud A., *Proximal radial artery ligation (PRAL) for reduction of flow in autogenous radial cephalic accesses for haemodialysis*, European Journal of Vascular and Endovascular Surgery, 2010, 40 (1), 94–99.

[6] Choi C.R., Kim C.N., *Analysis of blood flow interacted with leaflets in MHV in view of fluid-structure interaction*, Ksme International Journal, 2001, 15 (5), 613–622.

[7] Chung C.S., Karamanoglu M., Kovács S.J., *Duration of diastole and its phases as a function of heart rate during supine bicycle exercise*, AJP Heart and Circulatory Physiology, 2004, 287 (5), H2003–2008.

[8] Giersiepen M., Wurzinger L.J., Opitz R., Ma D., Mocco J., Hopkins L.N., *Estimation of shear stress-related blood damage in heart valve prostheses--in vitro comparison of 25 aortic valves*, The International Journal of Artificial Organs, 1990, 13 (5), 300–306.

[9] Hall A., Kovacs S., *Automated method for characterization of diastolic transmitral Doppler velocity contours: early rapid filling*, Ultrasound in Medicine and Biology, 1994, 20 (2), 107–116.

[10] Hall A.F., Aronovitz J.A., Nudelman S.P., Kovács S.J., *Automated method for characterization of diastolic transmitral Doppler velocity contours: Late atrial filling*, Ultrasound in Medicine and Biology, 1994, 20 (9), 859–869.

[11] Hayashida K., Lefèvre T., Chevalier B., Hovasse T., Romano M., Garot P., *Impact of Post-Procedural Aortic Regurgitation on Mortality After Transcatheter Aortic Valve Implantation*, Jacc Cardiovascular Interventions, 2012, 5 (12), 1247–1256.

[12] Heuser G., Opitz R., *A Couette viscometer for short time shearing of blood*, Biorheology, 1979, 17 (1–2), 17–24.

[13] Himburg H.A., *Spatial comparison between wall shear stress measures and porcine arterial endothelial permeability*, American Journal of Physiology-Heart and Circulatory Physiology, 2004, 286 (5), H1916–H1922.

[14] Honglong Y.U., Yuehu W.U., Feng X., Yuan H.E., Xie Q., Peng H.U., *Hemodynamic analysis of left ventricular unloading with Impella versus IABP during VA-ECMO*, Acta Bioeng. Biomech., 2024, 26 (2), 25–36.

[15] Jeong J.J., Hussain F., *On the identification of a vortex*, Journal of Fluid Mechanics, 1995, 332 (1), 339–363.

[16] Lantz J., Bck S., Carlhll C.J., Bolger A., Ebbers T., *Impact of prosthetic mitral valve orientation on the ventricular flow field: comparison using patient-specific Computational Fluid Dynamics*, Journal of Biomechanics, 2020, 116, 110209.

[17] Lehoux S., Castier Y., Tedgui A., *Molecular mechanisms of the vascular responses to haemodynamic forces*, Journal of Internal Medicine, 2006, 259 (4), 381–392.

[18] Machler H., Perthel M., Reiter G. et al., *Influence of bileafletprosthetic mitral valve orientation on left ventricular flow – anexperimental in vivo magnetic resonance imaging study*, European Journal of Cardio-Thoracic Surgery, 2004, 26 (4), 747–753.

[19] Makoto Kinoshita, Koutaro Yokote, Hidenori Arai, Mami Iida, Yasushi Ishigaki, Shun Ishibashi, *Japan Atherosclerosis Society (JAS) Guidelines for Prevention of Atherosclerotic Cardiovascular Diseases 2017*, Journal of Atherosclerosis and Thrombosis, 2018, 25 (9), 846–984.

[20] Murty R.S.V.N., Pabsetti P., Harish R., *CFD investigation of mechanical heart valve orientations in modulating left ventricular hemodynamics*, Results in Engineering, 2024, 24 (000).

[21] Patankar S.V., *Numerical heat transfer and fluid flow*, Series in Computational Methods in Mechanics and Thermal Sciences, 1980.

[22] Pawlikowski M., Nieroda A., *Comparative analyses of blood flow through mechanical trileaflet and bileaflet aortic valves*, Acta Bioeng. Biomech., 2022, 24 (2), 141–152.

[23] Qiang Y., Duan T., Zhang M., Qi L., Wei L., Zhong W., *Impact of bileaflet mechanical heart valve leaflet dysfunction on left ventricular blood flow: An experimental study*, Physics of Fluids, 2023, 35 (9), 091909.

[24] Qiang Y., Li Z., Zhang M., Duan T., Qi L., Wei L., *Effect of leaflet shape on the left ventricular blood flow pattern in BMHVs*, Experimental Thermal and Fluid Science, 2025, 161, 111343.

[25] Remuzzi A., *Disturbed flow in radial-cephalic arteriovenous fistulae for haemodialysis: low andoscillating shear stress locates the sites of stenosis*, Nephrology, Dialysis, Transplantation: of Ficialpublication of the European Dialysis and Transplant Association-European Renal Association, 2012, 27 (1), 358–368.

[26] Ruan C., Qi Y.U., Zhou J., Xinying O.U., Liu Y.I., Chen Y.U., *Fluid-structure interaction simulation for studying hemodynamics and rupture risk of patient-specific intracranial aneurysms*, Acta Bioeng. Biomech., 2023, 25 (3), 73–85.

[27] Issa R.I., *Solution of the implicitly discretised fluid flow equations by operator-splitting*, Journal of Computational Physics, 1991, 62 (1), 40–65.

[28] Sylvain, Laizet, Jovan, Nedi, Christos, Vassilicoset, *Influence of the spatial resolution on fine-scale features in DNS of turbulence generated by a single square grid*, International Journal of Computational Fluid Dynamics, 2015, 29 (3–5), 286–302.

[29] Szabó E., Baka E.Z., Tamás K., *Shear rate induced viscosity change of human blood samples and blood mimicking fluids*, Acta Bioeng. Biomech., 2024, 26 (1), 99–107.

[30] Throckmorton A.L., Ballman K.K., Myers C.D., Frankel S.H., Brown J.W., Rodefeld M.D., *Performance of a 3-bladed propeller pump to provide cavopulmonary assist in the failing fontan circulation*, Annals of Thoracic Surgery, 2008, 86 (4), 1343–1347.

[31] Vahanian A., Beyersdorf F., Praz F., Milojevic M., Zamorano J.L., *ESC/EACTS Guidelines for the management of valvular heart disease*, European Heart Journal, 2021, 43 (7), 561–632.

[32] Westerdale J.C., Adrian R., Squires K., Chaliki H., Belohlavek M., *Effects of Bileaflet Mechanical Mitral Valve Rotational Orientation on Left Ventricular Flow Conditions*, The Open Cardiovascular Medicine Journal, 2015, 9, 62–68.

[33] Xiang J., Natarajan S.K., Tremmel M., Ma D., Mocco J., Hopkins L.N., Siddiqui A.H., Levy E.I., Meng H., *Hemodynamic-morphologic discriminants for intracranial aneurysm rupture*, Stroke, 2011, 42 (1), 144–152.

[34] Xingshuang Ma, Hao Gao, Boyce E., *Image-based fluid–structure interaction model of the human mitral valve – ScienceDirect*, Computers and Fluids, 2013, 71 (1), 417–425.

[35] Yoganathan A.P., He Z., Casey Jones S., *Fluid Mechanics of Heart Valves*, Annual Review of Biomedical Engineering, 2004, 6 (1), 331–362.

[36] Zimmermann E., Schnapauff D., Dewey M., *Cardiac and Coronary Anatomy in Computed Tomography*, Semin. Ultrasound Ct Mr, 2008, 29 (3), 176–181.